

**THE USE OF SUBMODELS TO OPTIMIZE QUANTITATIVE PREDICTION ACCURACIES DERIVED FROM LASER-INDUCED BREAKDOWN SPECTRA.** K. H. Lepore, C. R. Ytsma, and M. D. Dyar, Mount Holyoke College, 50 College St., South Hadley, MA 01075.

**Introduction:** Laser-induced breakdown spectroscopy (LIBS) is an effective resource used to determine the geochemical composition of remote sites, as evidenced by the success of the ChemCam and SuperCam instruments onboard the *MSL Curiosity* [1,2,3] and *Perseverance* rovers [4,5,6,7], respectively. Because LIBS instruments can be operated remotely, this technique shows great potential for predicting the geochemistry of unknown targets on remote planetary bodies.

A key question for LIBS calibration efforts is how to optimize the selection of calibration standards used to predict the composition of an unknown target surface. Previous work has employed the use of “submodels”, in which a preliminary prediction of major element composition was used to group test spectra into low, mid and high concentration ranges [8]. Predictions were generated using models trained on spectra with matching concentrations.

In this study, we evaluate the effectiveness of various types of submodels by making direct comparisons among prediction accuracies calculated using spectra classified by  $\text{SiO}_2$  content only, by compositions of each major element, and by Si II/I ratios (a proxy for plasma temperature [9]). Our goal is to assess the merit of customizing LIBS calibration datasets to “match” the unknown targets by various means and establishes the best criteria to consider when choosing calibration spectra to optimize prediction accuracy.

**Methods:** Spectra were collected with the ChemLIBS instrument at the Mineral Spectroscopy Laboratory at Mount Holyoke College (MHC). The calibration suite at MHC includes 2990 rock powder standards collected from several sources with support from the NASA Mars Fundamental Research program [10]. Spectral preprocessing included dark subtraction, smoothing, wavelength alignment to a titanium standard, and correction for instrument response. Additional processing included normalization to the total intensity of each spectrometer range (UV, VIS, and VNIR) and application of a fully-automated baseline correction [11].

Partial-least square (PLS) models were generated and run on the Data Exploration, Visualization, and Analysis for Spectroscopy (DEVAS) website hosted by MHC (nemo.mtholyoke.edu). The entire calibration database was divided into training and test sets containing approximately 75% and 25% of all available spectra, respectively. Spectra used for submodels were selected from within these training and test sets.

*SiO<sub>2</sub> concentration-based submodels.* Training set spectra were sorted by known  $\text{SiO}_2$  concentration and separated into five ranges (Figure 1). Each submodel contained spectra collected from nearly 440 unique calibration standards. All training set spectra were used to generate preliminary  $\text{SiO}_2$  predictions (full-range) for all test spectra. Predicted  $\text{SiO}_2$  concentrations calculated using the full-range model were used to sort test spectra into the same five  $\text{SiO}_2$ -based ranges as training set spectra, each containing a similar number of reference targets ( $\approx 100$ -175). Submodels generated using training spectra sorted by known  $\text{SiO}_2$  concentrations were then used to make predictions for all major elements on test spectra in matching (predicted)  $\text{SiO}_2$  ranges.

*Si II/I ratio-based submodels.* Training and test set spectra were grouped by the ratio of the Si II emission line at 634.7 nm to the Si I line at 288.2 nm. Due to suspected inconsistencies in laser power as well as matrix effects from the complex plasmas arising from our geochemically diverse standards, these spectra represent a wide range of Si II/I ratios. Training set spectra were separated by Si II/I into five ranges with equal numbers of calibration spectra ( $\approx 440$ ). Models were used to predict major element compositions in the test spectra contained within each comparable Si II/I range.

*Blended submodels.* The complete training suite was used to calculate preliminary compositions for every major element. Test spectra were sorted by predicted composition of each major element and submodels with overlapping concentration ranges were used to produce a final prediction [8] (Figure 1). When initial predictions fell into an overlapping range between two submodels, a blended submodel was

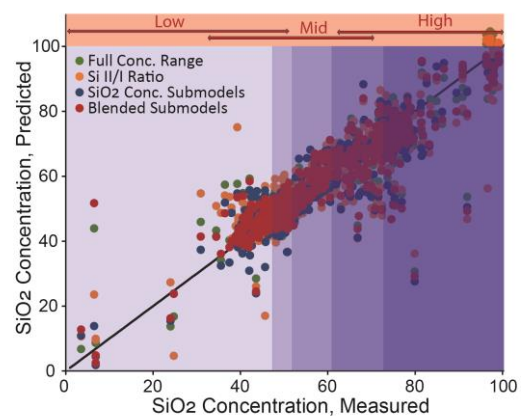


**Figure 1.** Predicted vs. measured  $\text{SiO}_2$  concentrations calculated using submodels and the full calibration database.

created using the weighted average of predictions from both submodels.

Prediction accuracies are reported as the root mean squared error of prediction (RMSE-P). Full model predictions employ the entire training and test sets (~2250 and ~750 calibration targets, respectively) for calibrations. In contrast, the total RMSE-P refers to a compilation of predicted and true compositions for all ranges within a submodel. This is similar to an average RMSE-P, but is appropriately weighted according to the number of calibration standards contained within each range.

**Conclusions:** A comparison among all submodels and full models indicates that separating spectra based on geochemical composition or plasma temperature

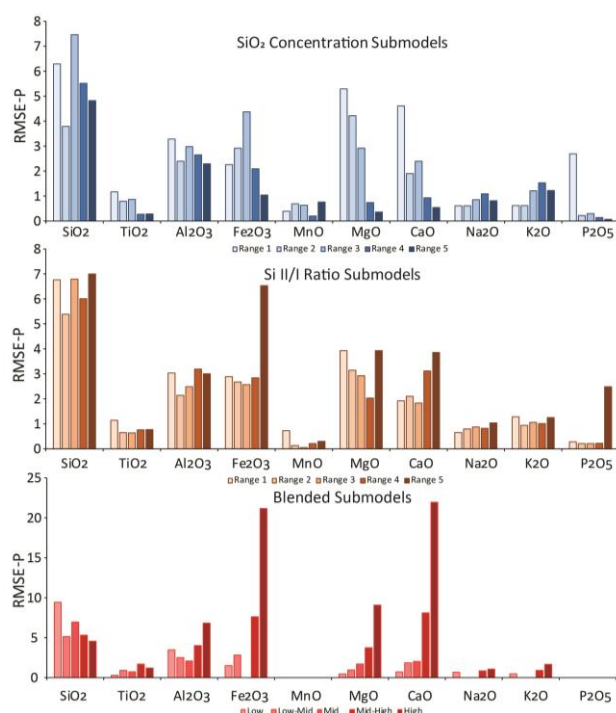


**Figure 2.** RMSE-Ps for each submodel method.

conditions can improve the accuracy of calibrations used to quantify the major element concentrations in unknown targets, but only under certain conditions. Advantages to using submodels are particularly evident within individual concentrations ranges, such as using high-SiO<sub>2</sub> standards to predict MgO and CaO compositions, or low-concentration MgO and CaO standards predicted using blended submodels (Figure 2). However, highly unreliable predictions can be generated using submodels, especially at extreme concentration ranges where few calibration standards are available for training and test sets. This is particularly evident in high-concentration Fe<sub>2</sub>O<sub>3</sub>, MgO, and CaO blended submodels.

Prediction accuracies for submodels are influenced by the size of the calibration suite, in addition to the ability of the training spectra to match the test spectra [12]. Because the ranges of the blended submodels are fixed according to concentration, the number of reference targets varies among elements' submodels in a way that reflects their composition distributions. This potentially complicates a direct comparison among submodel types.

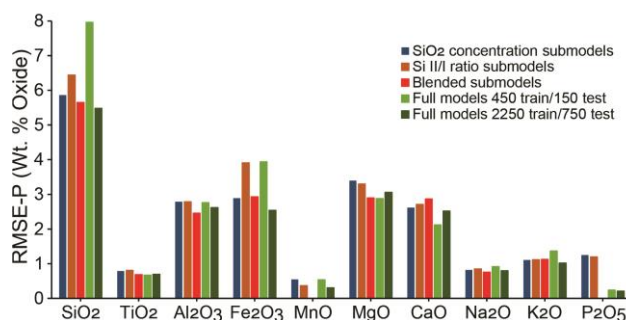


**Figure 3.** (top) Total RMSE-Ps for each submodel method used in this study.

A high degree of variability is observed among submodel ranges (Figure 2); however, the total RMSE-P can be used to gauge the overall accuracy of a submodel. No substantial differences in RMSE-P were found among total submodel and full model predictions (Figure 3). In fact, the full models presented here produced more accurate results than submodels for SiO<sub>2</sub>, Fe<sub>2</sub>O<sub>3</sub>, MnO, CaO, K<sub>2</sub>O, and P<sub>2</sub>O<sub>5</sub>. The implication is that unless the original dataset is large enough to support division into multiple submodels, the most accurate predictions are often generated by utilizing the greatest number of calibration standards available. Improved prediction accuracies of remote targets can be achieved through utilization of a large, geochemically diverse calibration database.

**Acknowledgments:** Supported by NASA grant NNN20ZDA001N.

**References:** [1] Wiens R. C. et al. (2012) *Space Sci. Rev.*, 170, 167-227. [2] Wiens R. C. et al. (2013) *Spectrochim. Acta B*, 82, 1-27. [3] Clegg S. (2017) *Spectrochim. Acta B*, 129, 64-85. [4] Wiens R. C. et al. (2020) *Space Sci. Rev.*, 217, 4. [5] Maurice S. et al. (2021) *Space Sci. Rev.*, 217, 47. [6] Manrique J. A. et al. (2020) *Space Sci. Rev.*, 216, 138. [7] Anderson, R. B. et al. (2021) *Spectrochim. Acta B*, DOI:10.1016/j.sab.2021.106347 [8] Anderson R. B. (2017) *Spectrochim. Acta B*, 129, 49-57. [9] Tokar R. L. (2015) *LPS XLVI*, Abstract #1369. [10] Dyar M. D. et al. (2019) *LPS L*, Abstract #1396. [11] Dyar M. D. et al. (2016) *Spectrochim. Acta B*, 126, 53-64. [12] Dyar M. D. and Ytsma, C. R. (2021) *Spectrochim. Acta B*, 177, 106073.